Robust Three-Phase Distribution System Frequency Measurement Using a Variable Step-Size LMS

Huilman S. Sanca, Flavio B. Costa, Francisco C. Souza Jr, Benemar A. de Souza.

***Abstract*—Frequency estimation is an important power quality parameter that is also useful for the protection and control of distributed generators. This paper proposes a robust three-phase distribution system frequency estimation algorithm based on the widely linear complex least mean square using a variable step-size to provide accurate frequency estimation and fast convergence during islanding of distributed generation (DG) and faults. The performance of the proposed method was evaluated in islanding events of DG. Besides, unbalanced analytical signals in amplitude and phase were evaluated as well as the impacts of the sampling rate and noise. The proposed algorithm was compared to other least mean square-based methods and good results were achieved.**

***Index Terms*—Least mean square, frequency estimation, unbalanced power system, distributed generation, islanding condition.**

I. Introduction

ESTIMATION of the correct fundamental frequency of the power distribution system is essential to perform protection and control actions, mitigate power quality problems and guarantee stable power system operation. Frequency measurement is a critical task in power distribution systems because of the increased number of non-linear loads which create different types and levels of voltage harmonics. Besides, the high penetration of distributed generation (DG) in the electric power distribution system has been increasing the complexity of the frequency estimation.

Several methods and techniques for frequency measurement have been developed by researchers. Traditionally, methods based on zero-crossing have been used to estimate the fundamental frequency because of their relative simplicity [1]. However, these methods are usually affected by harmonics and noise pollution. Methods based on the discrete Fourier transform (DFT) have been proposed [2]. These algorithms are immune to harmonic components and they have a relatively fast response time for the fundamental component calculation. However, the accuracy and convergence time of DFT-based algorithms are affected by the decaying DC component (DC offset), which can cause oscillations in the results [3].

Methods such as Kalman filtering [4], hybrid methods [5], adjustment of points to a sinusoidal waveform [6], [7], Newton-type algorithms [8], [9], adaptive notch filters [10], phase-locked loop [9], [11], least square (LS) [12], and nonlinear-LS [13] among others have been proposed for frequency estimation. However, almost all of these methods are based on the measurement of a single phase of the system, causing poor convergence when the tracked phase suffers a dip or a transient [14].

In three-phase power systems, just a single phase is not enough to characterize the whole system and its properties, especially under unbalanced three-phase systems. Therefore, methods based on a single-phase measurement of a system are limited in terms of system frequency characterization [14], [15], especially under unbalanced three-phase systems as well as under unbalanced faults. Therefore, a robust frequency estimator must take into account the information of all three-phase system voltages [16], [17].

Clarke's $\alpha\beta$ transformation maps the three-phase voltages onto α , β and zero voltage components, which can represent a complex-valued signal [18]. This complex signal from the $\alpha\beta$ transformation has been widely used by the least mean square (LMS) algorithm for three-phase signal frequency estimation [19], [20]. The LMS has been firstly introduced by Widrow and Hoff [18], [21] and different techniques based on LMS have been proposed due to the LMS algorithm, since it minimizes the instantaneous square error instead of the mean square error, using a simple gradient-based optimization method.

In [19], a widely linear (augmented) complex least mean square (ACLMS) based on the complex least mean square (CLMS) algorithm [22] was developed. From the unbalanced three-phase voltages, by the $\alpha\beta$ transformation, the widely linear modeling of the complex-valued signal was derived. However, algorithms such as LMS, CLMS, and ACLMS can present a poor convergence rate because the majority of these algorithms are analyzed with a fixed step size. The choice of the step size reflects a tradeoff between misadjustment and the speed of adaptation [23].

Considering unbalanced voltages, noises, and frequency deviation presented in the electric power system, this paper proposes an algorithm based on the ACLMS using a variable step-size instead of the fixed step-size to avoid poor convergence during power system disturbances. The performance of the proposed method was compared to the algorithms CLMS [22] and ACLMS [19] [20] for several critical cases, such as unbalance voltage (amplitude and phase), signals with noise pollution, islanding of DG, and fault inception and clearance. The IEEE 30 bus test system with DG was used in the simulation, and the performance of the proposed algorithm in terms of convergence and accuracy was superior in all the simulation cases compared to that of CLMS and ACLMS algorithms.

H. S. Sanca is with the Exact and Technological Sciences Center, Electrical Engineering, Federal University of Recôncavo da Bahia, Brazil. E-mail: huilman.sanca@ufrb.edu.br.

F. B. Costa is with School of Science and Technology, Federal University of Rio Grande do Norte, Brazil. E-mail: flaviocosta@ect.ufrn.br.

F. C. Souza Jr. is with the Federal Institute of Education, Science and Technology of Rio Grande do Norte, Brazil. E-mail: francisco.souza@ifrn.edu.br.

B. A. Souza is with the Department of Electrical Engineering, Federal University of Campina Grande, Brazil. E-mail: benemar@dee.ufcg.edu.br.

II. Variable Step-Size LMS

The LMS algorithm is described as follows:

$$W(k+1) = W(k) + \mu(k)e(k)x(k), \tag{1}$$

where $W(k)$ is the weight coefficient vector at the sampling k, μ is the step size, and $e(k)$ and $x(k)$ are the adaptation error and input vector, respectively, at the time instant k. In the case of the fixed step size $\mu(k)$ is chosen to be a constant. The majority of LMS algorithms considers a constant step-size μ [19], [20], [24]. The choice of the step size reflects a tradeoff between misadjustment and the speed of adaptation of LMS algorithms.

The variable step-size algorithms use a different step-size $\mu(k)$ for each adaptive filter coefficient, and the step-size is adjusted individually as adaptation progresses. These algorithms are more efficient than the LMS algorithms for coefficient tracking in nonstationary environments [23].

The variable step-size is updated as follows [25]:

$$\mu(k+1) = \alpha\mu(k) + \gamma p(k)^2, \tag{2}$$

where

$$p(k) = \beta p(k-1) + (1-\beta)[e(k)e(k-1) + e(k)^2], \tag{3}$$

where $0 < \alpha < 1$, $\gamma > 1$, $p(k)$ is the time-averaged estimation of the autocorrelation of $e(k)$ and $e(k-1)$, the positive constant β $(0 < \beta < 1)$ is an exponential weight parameter that governs the averaging time constant. $\mu(k+1)$ is set to μ_{max} or μ_{min} when it falls below or above the lower and upper boundaries, respectively.

III. Widely Linear Adaptive Filtering

A complex voltage can be written using the widely linear model as follows [19]:

$$v(k) = A(k)e^{j(\omega k\Delta T+\phi)} + B(k)e^{-j(\omega k\Delta T+\phi)} + z_{\alpha\beta}(k), \tag{4}$$

where,

$$A(k) = \frac{\sqrt{6}}{6}\left(V_a(k) + V_b(k) + V_c(k)\right),$$
$$B(k) = \frac{\sqrt{6}(2V_a(k) - V_b(k) - V_c(k))}{12} - \frac{\sqrt{2}(V_b(k) - V_c(k))}{4}j, \tag{5}$$

where $V_a(k)$, $V_b(k)$, and $V_c(k)$ are the instantaneous magnitude of each fundamental three-phase voltage component at the sampling k.

In unbalanced condition, $A(k)$ is no longer a constant, and $B(k) \neq 0$. Therefore, the coefficient of the widely linear model in (4) can be expressed using the ACLMS, given by [22]:

$$y(k+1) = \underbrace{v(k)h(k)}_{\text{standard update}} + \overbrace{v^*(k)g(k)}^{\text{conjugate update}}, \tag{6}$$

where $h(k)$ and $g(k)$ are filter weight coefficients updated at the instant associated to k and $*$ represents the complex conjugate.

From (4), the exact $v(k+1)$ can be obtained by:

$$\begin{aligned} v(k+1) &= A(k+1)e^{j\omega\Delta T}e^{j(\omega k\Delta T+\phi)} \\ &\quad + B(k+1)e^{-j\omega\Delta T}e^{-j(\omega k\Delta T+\phi)}, \end{aligned} \tag{7}$$

while from (4) and (6), the estimative $y(k+1)$ becomes:

$$\begin{aligned} y(k+1) &= A(k)h(k)e^{j(\omega k\Delta T+\phi)} + B(k)h(k)e^{-j(\omega k\Delta T+\phi)} \\ &\quad + A^*(k)g(k)e^{-j(\omega k\Delta T+\phi)} \\ &\quad + B^*(k)g(k)e^{j(\omega k\Delta T+\phi)} \\ &= [A(k)h(k) + B^*(k)g(k)]e^{j(\omega k\Delta T+\phi)} \\ &\quad + [A^*(k)g(k) + B(k)h(k)]e^{-j(\omega k\Delta T+\phi)}. \end{aligned} \tag{8}$$

The error $e(k)$ between the exact $v(k+1)$ and the estimated $y(k+1)$ values can be obtained by:

$$\begin{aligned} e(k) &= v(k+1) - y(k+1) \\ &= v(k+1) - v(k)h(k) - v^*(k)g(k) \end{aligned} \tag{9}$$

where

$$\begin{aligned} h(k+1) &= h(k) + \mu e(k)v^*(k) \\ g(k+1) &= g(k) + \mu e(k)v(k) \end{aligned} \tag{10}$$

where $h(k)$ and $g(k)$ are respectively the filter weight coefficients corresponding to the standard and conjugate parts at the sampling k, and μ is the fixed step-size, a small positive constant [19].

IV. The Proposed Method for Unbalanced Three-phase Power System

The instantaneous three-phase voltages of a power system can be represented in the discrete time form as follows:

$$\begin{aligned} v_a(k) &= V_a(k)\cos(\omega k\Delta T + \phi) + \eta_a(k), \\ v_b(k) &= V_b(k)\cos\left(\omega k\Delta T + \phi - \frac{2\pi}{3} + \Delta_b\right) + \eta_b(k), \\ v_c(k) &= V_c(k)\cos\left(\omega k\Delta T + \phi + \frac{2\pi}{3} + \Delta_c\right) + \eta_c(k), \end{aligned} \tag{11}$$

where $\omega = 2\pi f_0$ is the angular frequency of the voltage and f_0 the fundamental frequency, $\Delta T = 1/f_s$ is the sampling interval, f_s is the sampling frequency, ϕ denotes the phase of the fundamental component, while η_a, η_b and η_c are noise of the signal, and Δ_b and Δ_c represent the phase deviation.

The three-phase voltages in (11) are routinely transformed by the Clarke's transform, known as the orthogonal $\alpha\beta0$ transformation matrix, to the zero-sequence v_0 and direct and quadrature-axis components, v_α and v_β, as follows [15], [18]:

$$\begin{bmatrix} v_0(k) \\ v_\alpha(k) \\ v_\beta(k) \end{bmatrix} = \mathbf{C}_{\alpha\beta0} \begin{bmatrix} v_a(k) \\ v_b(k) \\ v_c(k) \end{bmatrix} \Longleftrightarrow \mathbf{A}_{\alpha\beta0} = \mathbf{C}_{\alpha\beta0}\mathbf{A}_{abc}, \tag{12}$$

where,

$$\mathbf{C}_{\alpha\beta0} = \sqrt{\frac{2}{3}}\begin{bmatrix} \frac{\sqrt{2}}{2} & \frac{\sqrt{2}}{2} & \frac{\sqrt{2}}{2} \\ 1 & -\frac{1}{2} & -\frac{1}{2} \\ 0 & \frac{\sqrt{3}}{2} & -\frac{\sqrt{3}}{2} \end{bmatrix}, \tag{13}$$

where $\mathbf{A}_{abc}$ represents the three-phase signal voltages, $\mathbf{A}_{\alpha\beta0}$ represents the direct and quadrature-axis components and the zero-sequence. The constant $\sqrt{2/3}$ is used to guarantee that the system is invariant under this transformation. In balanced power system, the voltage amplitudes are identical, $V_a(k) = V_b(k) = V_c(k)$ and $\Delta_b = \Delta_c = 0$, so that the voltage signals v_α and v_β can be written as follows:

$$\begin{aligned} v_\alpha(k) &= A(k)\cos(\omega k\Delta T + \phi) + \eta_\alpha(k), \\ v_\beta(k) &= A(k)\cos(\omega k\Delta T + \phi + \frac{\pi}{2}) + \eta_\beta(k), \end{aligned}$$

where $v_0(k) = 0$ and $A(k) = \sqrt{6/2}V_a(k)$. Via $\alpha\beta 0$ transformation the mapped noise can be denoted by:

$$\eta_\alpha(k) = \sqrt{\frac{2}{3}}\left(\eta_a(k) - \frac{1}{2}\eta_b(k) - \frac{1}{2}\eta_c(k)\right),$$

$$\eta_\beta(k) = \sqrt{\frac{2}{3}}\left(\frac{\sqrt{3}}{2}\eta_b(k) - \frac{\sqrt{3}}{2}\eta_c(k)\right).$$

In practice, only the components v_α and v_β are used [19]. Using the $\alpha\beta$ transformation, it is possible to obtain the complex voltage signal $v(k)$ of the system, which serves as a desired signal in the adaptive frequency estimation given by:

$$v(k) = v_\alpha + jv_\beta. \tag{14}$$

In normal operating conditions, the trajectory of samples $v(k)$ becomes a perfect circle in the $\alpha\beta$ plane, as shown in Fig 1. In the case of the circular vector trajectory, the frequency estimation can be performed adequately by traditional frequency estimation algorithms such as the CLMS designed for balanced power systems.

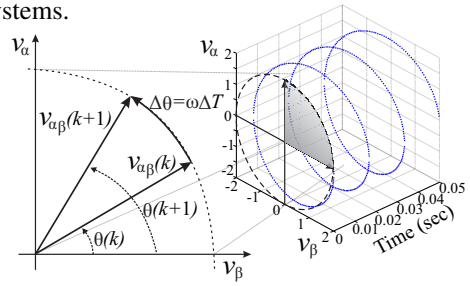

Fig. 1. Circularity via $\alpha\beta$ scatter plot. Voltage vector trajectory in two-phase $\alpha\beta$ complex plane. The circular complex-valued trajectory obtained from a balanced situation where $V_a(k)$, $V_b(k)$ and $V_c(k)$ are identical at 1p.u.

The three-phase system can be transformed into a two-phase complex one using (12), resulting in the complex voltage vector (14), which can be iteratively estimated by:

$$\begin{aligned} v(k+1) &= A(k+1)e^{j(\omega(k+1)\Delta T+\phi)} + \eta_{\alpha\beta}(k+1) \\ &= A(k+1)e^{j\omega\Delta T}e^{j(\omega k\Delta T+\phi)} + \eta_{\alpha\beta}(k+1) \\ &= v(k)e^{j\omega\Delta T} + \eta_{\alpha\beta}(k+1), \end{aligned} \tag{15}$$

where $\eta_{\alpha\beta}(k+1) = \eta_\alpha(k+1) + j\eta_\beta(k+1)$. However, in real cases, when the three-phase power system deviates from its normal condition such as in voltage sags, when the three-phase voltage amplitudes are not identical, $V_a(k) \neq V_b(k) \neq V_c(k)$ or if $\Delta_b = \Delta_c = 0$ is not satisfied, the system trajectory of $v(k)$ on the plane $\alpha\beta$ becomes noncircular. For this case, the widely linear model can be used and the complex voltage in (14) can be written in the format of (4).

In the widely linear model, the weight coefficients h_k and g_k described in (6) and (10), which use the step-size μ as a constant, are obtained. However, when μ is considered constant, the algorithm suffers from the problem of poor convergence rate during an unbalanced situation on the power system.

Applying (2) and (3) in (10), for the new weight vector coefficients $h(k)$ and $g(k)$, respectively, hence, both $h(k)$ and $g(k)$ weight coefficients corresponding to the standard and conjugate parts at the sampling k in (6) can be written in the recursive form as follows:

$$\begin{aligned} h(k) &= h(k-1) + \mu(k)e(k-1)v^*(k-1), \\ g(k) &= g(k-1) + \mu(k)e(k-1)v(k-1), \end{aligned} \tag{16}$$

where $\mu(k)$ is the variable step-size known as the convergence factor, which controls the stability and rate of the convergence of the algorithm at the sampling k. Different to the traditional methods proposed in [1], [19], [20], [22], [24], this paper proposes the use of (2) for better convergence and noise immunity. The variable step-size $\mu(k)$ in the recursive is be given by:

$$\mu(k) = \alpha\mu(k-1) + \gamma p(k)p(k)^*, \tag{17}$$

where

$$p(k) = \beta p(k-1) + (1-\beta)\{e(k)[e(k-1) + e(k)]\}. \tag{18}$$

Considering (1) for the weight vectors $h(k)$ and $g(k)$ in unbalanced three-phase power systems, the variable step-size $\mu(k)$ is given by:

$$\mu(k) = \begin{cases} \mu_{max}, & \text{if} \quad \mu(k) > \mu_{max}, \\ \mu_{min}, & \text{if} \quad \mu(k) < \mu_{min}, \\ \mu(k), & \text{otherwise} \quad , \end{cases} \tag{19}$$

where $\mu(0) = \mu_{max}$ and $p(0) = \mu(0)$. In widely linear analysis, $v(k+1) \simeq y(k+1)$, $A(k+1) \simeq A(k)$ and $B(k+1) \simeq B(k)$ are considered to estimate the instantaneous frequency of the system. Therefore, the coefficient of the terms $e^{j(\omega k\Delta T+\phi)}$ and $e^{-j(\omega k\Delta T+\phi)}$ in (8) and (7) are compared, and the phasor term that contains the frequency information is obtained by:

$$[A(k)h(k) + B^*(k)g(k)] = A(k)e^{j\omega\Delta T} \tag{20}$$

and

$$[A^*(k)g(k) + B(k)h(k)] = B(k)e^{-j\omega\Delta T}, \tag{21}$$

where

$$e^{j\omega\Delta T} = h(k) + \frac{B^*(k)}{A(k)}g(k), \tag{22}$$

$$e^{-j\omega\Delta T} = h(k) + \frac{A^*(k)}{B(k)}g(k). \tag{23}$$

Conjugating (23) and substituting in (22), considering $m(k) = \frac{B^*(k)}{A(k)}$, the following quadratic equation is obtained:

$$g(k)m^2(k) + (h(k) - h^*(k))m(k) - g*(k) = 0. \tag{24}$$

Solving (24), the two roots are given by:

$$m_1(k) = \frac{-j\Im m(h(k)) + j\sqrt{\Im m^2(h(k)) - |g(k)|^2}}{g(k)}, \tag{25}$$

$$m_2(k) = \frac{-j\Im m(h(k)) - j\sqrt{\Im m^2(h(k)) - |g(k)|^2}}{g(k)}, \tag{26}$$

where the operator $\Im m(.)$ represents the imaginary part of the complex-valued number.

Considering $m_1(k)$ and $m_2(k)$, the phasor $e^{j\omega\Delta T}$ may be estimated by using $h(k) + m_1(k)g(k)$ or $h(k) + m_2(k)g(k)$. The imaginary part of $e^{j\omega\Delta T}$ is positive because the system frequency is smaller than the sampling frequency and, for this, the solution based on $m_2(k)$ can be excluded [19].

Finally, the frequency $\widehat{f}(k)$ is estimated from the term $e^{j\omega\Delta T}$ as follows:

$$\widehat{f}(k) = \frac{1}{2\pi\Delta T}\sin^{-1}(\Im m(h(k) + m_1(k)g(k))). \tag{27}$$

Fig. 2 depicts the flowchart of the proposed algorithm, which is executed at each sampling time, with the following description:

1) Input signals, which are three-phase voltages.

2) The complex voltage signal $v_{(k)}$ of the system is obtained from the $\alpha\beta$ transformation.
3) The parameter $\mu(k)$ described in Table I is redefined.
4) The widely linear adaptive filtering is used.
5) The variable step size is calculated and compared to the maximum and minimum $\mu(k)$ to be used in the next step.
6) The weight coefficients are computed based on $\mu(k)$.
7) The quadratic equation is solved to obtain two roots.
8) One of the roots is used and the frequency of the system is finally calculated.

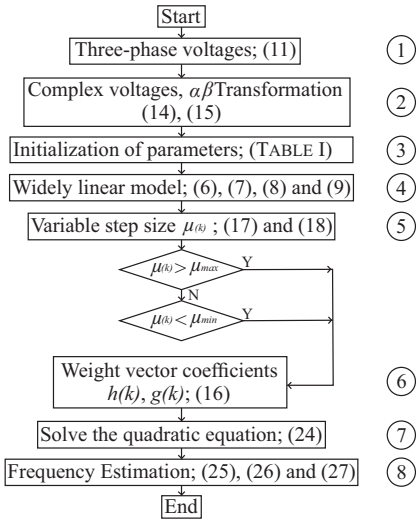

Fig. 2. Flowchart of proposed frequency estimation method.

V. Performance Assessment with Analytical Signals

The performance of the proposed algorithm was evaluated through analytical signals, where the exact frequency contents are known, and comparisons to the CLMS and ACLMS methods were accomplished. The parameter used by the methods CLMS and ACMLS is $\mu = 0.01$, whereas the proposed method requires the parameters summarized in Table I [19] [25].

TABLE I
Parameters used for test and simulations studies of the proposed technique.

Algorithm	Parameter	Value
Proposed	Initial μ	μ_{max}
	Initial p	Initial μ
	γ	0.08
	α	0.97
	β	0.99
	μ_{max}	0.01
	μ_{min}	0.001

A. Unbalanced signal

Table II summarizes the parameters of the analytical signals with fundamental frequency of $f = 50$ Hz and sampling frequency of $f_s = 5$ kHz (100 samples per cycle). In case I, the signal is unbalanced in magnitude, whereas in case II the signals are unbalanced in both magnitude and phase. Fig. 3 presents the performance of CLMS, ACLMS, and the proposed algorithms for estimating the fundamental frequency of the analytical signals. Therefore, under unbalanced conditions, the frequency estimated by the CLMS algorithm presented an oscillatory steady-state and poor convergence, whereas the proposed algorithm and the ACLMS achieved good performance with disregarded oscillations around the correct frequency value.

TABLE II
Simulation Cases with Analytical Signals.

Case	$V_a(p.u.)$	$V_b(p.u.)$	$V_c(p.u.)$	Δ_b	Δ_c
I	0.6	1	1	-5°	5°
II	0.6	0.7	0.7	-10°	10°

B. Effects of the sampling frequency and noise

The boxplots in Fig.4 presents the performance of the CLMS, ACLMS, and the proposed algorithms considering the unbalanced signals with Signal-to-Noise Ratio (SNR) of 20, 40, and 60 dB and sampling frequency of 5 and 20 kHz.

The proposed algorithm presented the best performance in all cases. Conversely, the CLMS presented poor convergence to estimate the fundamental frequency due to the unbalanced signals.

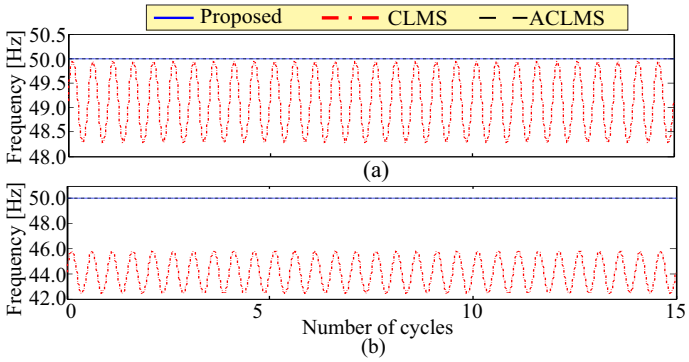

Fig. 3. Frequency estimation under unbalanced conditions: (a) Case I, (b) Case II.

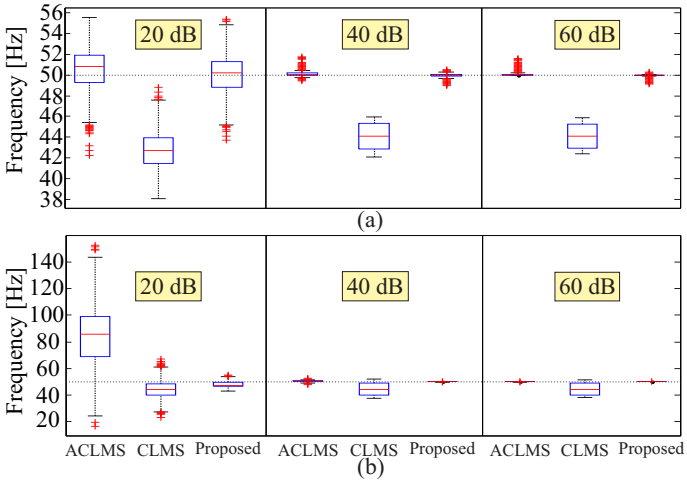

Fig. 4. Performance of the fundamental frequency estimation under SNR of 20, 40 and 60 dB: (a) $f_s = 5$ kHz (N=100 samples/cycle); (b) $f_s = 20$ kHz (N=400 samples/cycle).

Regarding the noise effects, both the proposed method and the ACLMS presented the best results for SNR of 60 and 40 dB. Besides, by using a sampling frequency of 20 kHz, the proposed method presented good results for SNR of 20 dB, which would be a critical situation with a high polluted noise level. Conversely, the ACLMS method was affected by

low SNR. The CLMS method was the highest affected by the noise.

Regarding the sampling frequency, all methods presented the best performance for 20 kHz except for the ACLMS with low SNR. Conventional protective relays have used low sampling frequency for estimating the frequency and other parameters from voltage and current phasors. However, with the advent of the smart grids high-speed protective functions with sampling frequency in the order of some kHz have been proposed [26]. Besides protection, digital fault recorders usually use a sampling frequency of the order of 20 kHz. Also, a sampling frequency of some kHz is usual for power system control applications such as the control of synchronous machines. Therefore, the sampling frequency of 5 or 20 kHz is possible in actual applications.

VI. Performance Assessment with Simulations from an Electric Power System

Fig. 5 depicts the IEEE 30-bus test power system, which parameters are available in [27]. This power system is

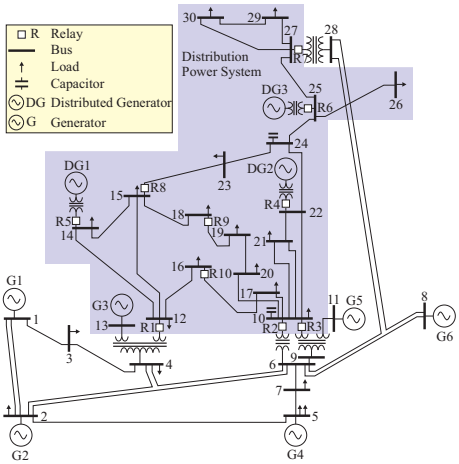

Fig. 5. Single-line diagram of the IEEE 30-bus power system with DG [27] [28]

composed of 37 lines, 6 generators, and 4 transformers (sub-transmission system at 132 kV and distribution system at 33 kV). Also, three synchronous generators (DG1,DG2, and DG3) of 20 MVA were used as DG and connected at buses 14, 22 and 25, respectively. The parameters of the synchronous generator are available in [28]. The monitoring points were at these buses. The fundamental frequency is f=50 Hz and the sampling frequency is $f_s = 5$ kHz.

The accurate estimation of the frequency is a key point for the protection and control of distributed generators. For instance, depending on the local standards, the distributed generator must be disconnected if the frequency is out of specific thresholds during a specific time. In a 50 Hz system, the relays of frequency variation (ROCOF relays) are typically set between 0.1 and 1.0 Hz and the operating time is between 0.2 and 0.5 s. [29]. The ROCOF relay was not implemented, but the results are explained in this context, and thresholds of 50 $\pm$0.5 Hz were selected for the sake of illustration.

A. Islanding of Distributed Generation

An islanding operation occurs when the DG continues supplying power to a portion of the network (islanded network) after power from the main utility or power substations are interrupted. This situation can cause low-frequency oscillation in voltage, current, and frequency of the islanded synchronous generators due to the power loss of the main sources, especially when the power of the DG is not enough to supply the islanded loads [30].

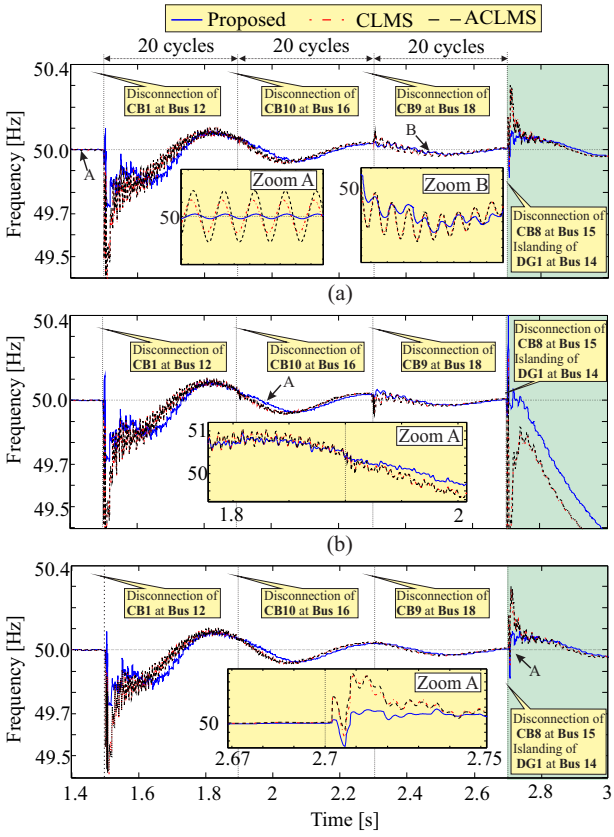

Fig. 6. Frequency estimation in the distribution system with distributed generation in islanding operation for $f_s = 5$ kHz. Monitoring at: (a) bus 22; (b) bus 14; (c) bus 25.

An islanding situation was simulated by opening the circuit breakers CB1, CB8, CB9, and CB10 in Fig. 5. In this case, the DG1 with a power of 20 MVA was islanded and would supply a total load of 35.32 MVA. Therefore, it is expected a low-frequency oscillation on the frequency during the islanding process followed by a loss of synchronism after the islanding [29]. Hence, a ROCOF relay would disconnect such a generator. Conversely, the other DGs connected to the grid would not present loss of stability, just low-frequency oscillations on the estimated frequency.

Fig. 6 depicts the performance of the frequency estimation-based algorithms (CLMS, ACLMS, and the proposed method), by using a sampling frequency of 5 kHz, whereas Fig. 7 depicts the same islanding situation with algorithms sampled at 20 kHz.

According to Fig. 6, the estimated frequency with CLMS and ACLMS algorithms were subject to a hard high-frequency oscillation superimposed to the low-frequency oscillation during the disconnection at bus 12, which is not islanding yet. Also, the estimated frequency exceeded the lower threshold of 49.5 Hz, which would subject the ROCOF relay to misop-

erate depending on the settings. Therefore, the relay could disconnect the DGs during switching operations wrongly. The frequency estimated by the proposed method did not present considerable high-frequency oscillations instability and did not cross the frequency thresholds during the switching operations on the power stations. Therefore, no distributed generator would be disconnected from the switching at the substation. The islanding is accomplished from the disconnection of CB8 at bus 15 and only the generator DG1 is islanded as aforementioned. By using the proposed method, only the right distributed generator (DG1) would be disconnected by a ROCOF relay soon after the islanding process because the estimated frequency indicates the loss of synchronism (Fig. 6b).

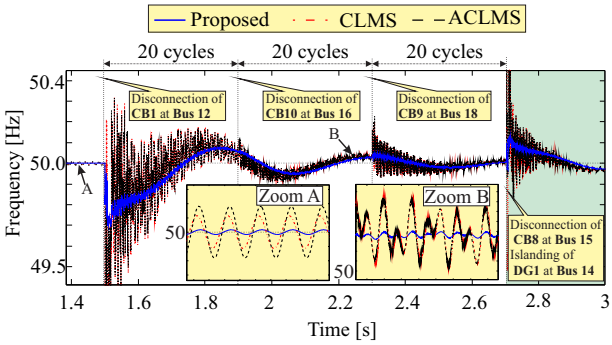

Fig. 7. Frequency estimation in the distribution system with distributed generation in islanding operation for $f_s = 20$ kHz. Monitoring at bus 22.

The CLMS and ACLMS methods were affected by a higher sampling rate (20 kHz), presenting considerable high-frequency oscillations (Fig. 7). The proposed algorithm presented the best performance, demonstrating that it is scarcely affected by a higher sampling frequency.

B. Unintentional Islanding of Distributed generation due to Faults

Unintentional islanding of DG must be prevented due to various risks and problems, such as work or public safety, equipment damage, unacceptable supply voltage/frequency, etc. [31]. Additionally, without strict frequency control, the balance between load and generation in the islanded area is going to be violated, leading to abnormal frequencies and voltages. A result of missing control in islanding situation might be the frequency oscillation which represents a high risk for machines and drives [32].

Unintentional islanding is usually the consequence of a fault in the network. When a fault takes place on the power system, the protective devices must isolate the faulted area as soon as possible while maintaining service continuity in the rest of the system. i.e., the generators should not be disconnected, just the faulted areas must be isolated. However, if a distributed generator is placed inside the isolated area with fault, it must be disconnected as soon as the island formation. Therefore, the protection of the distribution system with distributed generation has become a challenge.

With distributed generation, the over-current protective relays tend to be less sensitized due to several power sources. In addition, if the overcurrent protective devices trip correctly, distributed generations can feed the fault and anti-islanding procedures must be considered. In this context, the frequency is one of the most important parameters used by distributed generators to prevent undesirable islanding during faults.

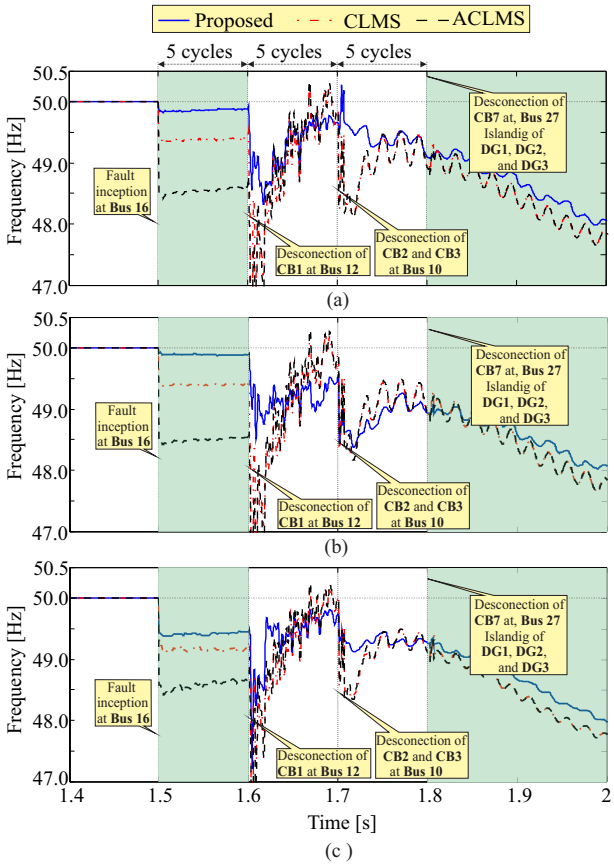

Fig. 8. Frequency estimation in the distribution system with distributed generation during a three-phase fault followed by unintentional islanding. Monitoring at: (a) bus 22; (b) bus 14; (c) bus 25.

This situation was reproduced in the power system of Fig. 4 through a severe three-phase short circuit at bus 16. The circuit-breakers opened at 100 ms (CB1), 200 ms (CB2 and CB3), and 300 ms (CB7) (5, 10, and 15 cycles) after the fault inception time, respectively, to protect the substations.

This sequence of events emulates a cascade event due to a permanent fault in a hypothetical situation where there is only over-current protection on the substations and considering the sequential trip assuming highest over-current for the nearest buses of the fault.

Fig. 8 depicts the performance of the frequency estimation-based algorithms (CLMS, ACLMS, and the proposed methods) during the unintentional islanding.

Regarding the first five cycles of the fault, where the circuit-breakers of the substations were not opened yet, the frequency deviation is not expected to be high. The CLMS and ACLMS methods presented a high deviation of the frequency over the frequency thresholds, which would cause improper disconnection of the DG units. Conversely, the frequency estimated by the proposed method did not cross the frequency thresholds, which would not cause wrongly disconnection of DG during the beginning of the fault. When the power substations start the disconnections, i.e., the distributed generators start to be

islanded due to the fault, such generators lose the control and stability, and all methods indicate this situation. Therefore, the distributed generators would be disconnected. However, the proposed method presented the best convergence with the smallest oscillation in the frequency estimation.

C. Islanding Situations with Different Nominal Power

This section presents the performance assessment of the frequency estimation methods in challenging situations, which are islanding situations with DG sources with different nominal power. The islanding of DG was accomplished with the DG sources with 20%, 40%, 60%, 80%, and 100% of the nominal power.

The performance of the methods was assessed considering the relative error given by:

$$Relative\ error[\%] = \frac{\left|f_{ref} - \hat{f}\right|}{f_{ref}} 100, \tag{28}$$

were f_{ref} is the reference frequency of the system, obtained directly from the generator shaft, in rad/s, and then converted to Hz by the constant 0.1559155.

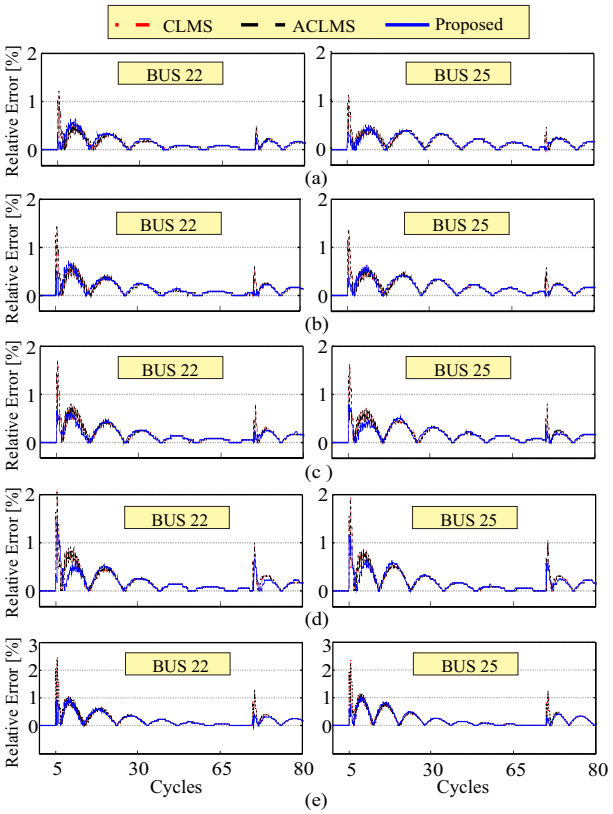

Fig. 9. Relative errors of the frequency estimation methods during islandings with DGs with different power: (a) 20%, (b) 40%, (c) 60%, (d) 80% and (e) 100%.

Fig. 9 depicts the relative error in the frequency estimation with monitoring points located in the busses 22 and 25. The proposed method presented the best performance with 0.5% average errors less than the other methods in the cases shown in Figs. 9(a), (b), (c). In the cases with DG power with 80% and 100%, the proposed method presented peaks with errors up to 1% because of the greater the variation in power, the greater the oscillation in the frequency estimation during an islanding situation. These cases are considered the most undesirable in distribution systems with DG. The other methods presented larger errors than the proposed one in these severe cases.

D. Computational Burden of the Proposed method

The number of floating-point operations (FLOPs) required by the proposed algorithm is an important parameter to verify if it is feasible to be implemented in hardware for a real-time evaluation in a practical application. Considering the sampling frequency of f_s=15360 Hz, the computational burden necessary for calculating Eqs. (6)-(9), (14), (15), (17), and (18), per sampling time of 65 μs, is 1297 sums, 2073 multiplications, 2 divisions, 5 square roots, and 2 power operations. The number of FLOPs required to run these mathematical algorithms can change with the used DSP. Based on [33], the computational burden of the proposed method would be approximately 3460 FLOPs to be accomplished in 65 μs.

Modern DSP runs million FLOPs per second (MFLOPS). For instance, the DSP TMS320C6748 performs up to 2746 MFLOPS [33]. Therefore, it performs up to 178.490 FLOPs in 65 μs, which is more than that required by the proposed method. For instance, the proposed method with a computational burden of approximately 3460 FLOPs would be executed in about 1.26 μs, which is much less than 65 μs. Therefore, the proposed method could be implemented in the DSP TMS320C6748 to perform a real-time evaluation of the fundamental frequency at a sampling frequency of 15360 Hz.

VII. Performance Assessment with an Actual Disturbance

Fig. 10 depicts a measurement from an actual 230 kV, 60 Hz, Brazilian transmission line, which was recorded at a sampling frequency of 15360 Hz. This measurement recorded a voltage sag due to a single phase-to-ground fault at phase C with a duration of about three cycles. The frequency estimated by the proposed method and the methods CMLS and ACMLS are also shown in Fig. 10.

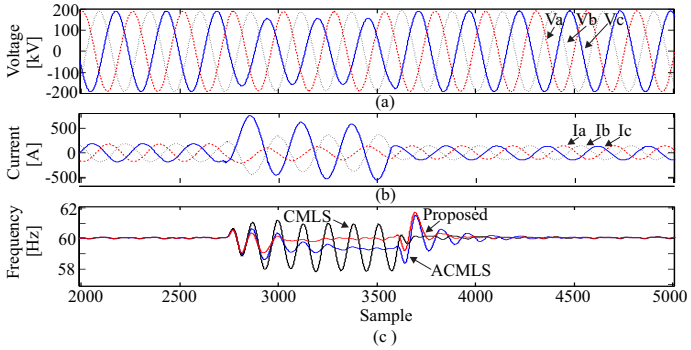

Fig. 10. Actual record with a voltage sag: (a) voltages, (b) currents, (c) Frequency estimations.

According to the estimated frequencies in Fig. 10(C), the proposed method presented an effective frequency estimation

with fewer oscillations than the methods ACLMS and CMLS. These results confirm the good performance and robustness of the proposed method for frequency estimation.

VIII. Conclusion

This paper presented a frequency estimation algorithm based on the widely linear complex least mean square with a variable step-size to estimate instantaneous frequency in a three-phase power system. The proposed algorithm was compared to the CLMS and ACLMS algorithms.

The proposed method was evaluated with analytical unbalanced signals with different noises and sampling frequencies. The proposed algorithm presented the best performance and the fastest convergence, which demonstrated the robustness of the proposed algorithm.

The performance of the proposed algorithm was also evaluated with simulated signals from a distribution power system with distributed generation under islanding situations and an actual measurement in a Brazilian transmission line during a fault. The proposed algorithm presented good performance during the dynamic changes in the power system, and the accuracy of the frequency estimation was satisfactory even in the presence of islanding situations, voltage sags, and faults due to the used variable step-size. Conversely, the CLMS and ACLMS algorithms would wrongly disconnect the distributed generators in some situations if they would be used in a frequency relay. In the evaluation of the actual case, the proposed method obtained good results, confirming its efficiency and robustness for the frequency estimation.

References

[1] Y. Xia, Z. Blazic, and D. P. Mandic, "Complex-valued least squares frequency estimation for unbalanced power systems," *IEEE Transactions on Instrumentation and Measurement*, vol. 64, no. 3, pp. 638–648, March 2015.

[2] Candan, "Analysis and further improvement of fine resolution frequency estimation method from three dft samples," *IEEE Signal Processing Letters*, vol. 20, no. 9, pp. 913–916, 2013.

[3] Y. S. Cho, C. K. Lee, G. Jang, and H. J. Lee, "An innovative decaying dc component estimation algorithm for digital relaying," *IEEE Transactions on Power Delivery*, vol. 24, no. 1, pp. 73–78, Jan 2009.

[4] A. Routray, A. K. Pradhan, and K. P. Rao, "A novel kalman filter for frequency estimation of distorted signals in power systems," *IEEE Transactions on Instrumentation and Measurement*, vol. 51, no. 3, pp. 469–479, Jun 2002.

[5] R. A. Zadeh, A. Ghosh, G. Ledwich, and F. Zare, "Analysis of phasor measurement method in tracking the power frequency of distorted signals," *IET Generation, Transmission Distribution*, vol. 4, no. 7, pp. 759–769, July 2010.

[6] E. Sorrentino, R. Carvalho, R. Carvalho, R. Carvalho, and R. Carvalho, "Performance of three algorithms for frequency measurement under transient conditions," *Electric Power System Research*, vol. 80, pp. 1191–1196, Mar. 2010.

[7] SOUZA JR. F. C., SANCA H. S., SOUZA B. A. e COSTA, F. B, "Adaptive instantaneous overcurrent relay settings in real brazilian system with distributed generation," *International Journal of Scientific and Engineering Research - IJSER*, vol. 7, no. 10, pp. 1708–1714, 2016.

[8] I. Sadinezhad and V. G. Agelidis, "Slow sampling online optimization approach to estimate power system frequency," *IEEE Transactions on Smart Grid*, vol. 2, no. 2, pp. 265–277, June 2011.

[9] M. S. Reza, M. Ciobotaru, and V. G. Agelidis, "Power system frequency estimation by using a newton-type technique for smart meters," *IEEE Transactions on Instrumentation and Measurement*, vol. 64, no. 3, pp. 615–624, March 2015.

[10] M. Meller, "Frequency guided generalized adaptive notch filtering 2014 tracking analysis and optimization," *IEEE Transactions on Signal Processing*, vol. 63, no. 22, pp. 6003–6012, Nov 2015.

[11] F. Wu, L. Zhang, and J. Duan, "Effect of adding dc-offset estimation integrators in there-phase enhanced phase-locked loop on dynamic performance and alternative scheme," *IET Power Electronics*, vol. 8, no. 3, pp. 391–400, 2015.

[12] M. D. Kusljevic, "On ls-based power frequency estimation algorithms," *IEEE Transactions on Instrumentation and Measurement*, vol. 62, no. 7, pp. 2020–2028, 2013.

[13] R. Chudamani, K. Vasudevan, and C. S. Ramalingam, "Real-time estimation of power system frequency using nonlinear least squares," *IEEE Transactions on Power Delivery*, vol. 24, no. 3, pp. 1021–1028, July 2009.

[14] M. M. Canteli, A. O. Fernandez, L. I. Eguiluz, and C. R. Estebanez, "Three-phase adaptive frequency measurement based on clarke's transformation," *IEEE Transactions on Power Delivery*, vol. 21, no. 3, pp. 1101–1105, July 2006.

[15] V. Eckhardt, P. Hippe, and G. Hosemann, "Dynamic measuring of frequency and frequency oscillations in multiphase power systems," *IEEE Transactions on Power Delivery*, vol. 4, no. 1, pp. 95–102, Jan 1989.

[16] M. Mojiri, D. Yazdani, and A. Bakhshai, "Robust adaptive frequency estimation of three-phase power systems," *IEEE Transactions on Instrumentation and Measurement*, vol. 59, no. 7, pp. 1793–1802, July 2010.

[17] A. Khalili, A. Rastegarnia, and S. Sanei, "Robust frequency estimation in three-phase power systems using correntropy-based adaptive filter," *IET Science, Measurement Technology*, vol. 9, no. 8, pp. 928–935, 2015.

[18] A. K. Pradhan, A. Routray, and A. Basak, "Power system frequency estimation using least mean square technique," *IEEE Transactions on Power Delivery*, vol. 20, no. 3, pp. 1812–1816, 2005.

[19] Y. Xia, S. C. Douglas, and D. P. Mandic, "Adaptive frequency estimation in smart grid applications: Exploiting noncircularity and widely linear adaptive estimators," *IEEE Signal Processing Magazine*, vol. 29, no. 5, pp. 44–54, 2012.

[20] ——, "Adaptive frequency estimation in smart grid applications: Exploiting noncircularity and widely linear adaptive estimators," *IEEE Signal Processing Magazine*, vol. 29, no. 5, pp. 44–54, Sept 2012.

[21] B. Widrow and M. E. Hoff Jr., "Adaptive switching circuits," *Stanford Electron Labs, Stanford, CA*, pp. 1–9, 1960.

[22] S. Javidi, M. Pedzisz, S. L. Goh, and D. P. Mandic, "The augmented complex least mean square algorithm with application to adaptive prediction problems," *In Proc. 1st IARP Workshop Cong. Infrm. Process, Santorini, Greece*, pp. 54–54, 2008.

[23] T. Aboulnasr and K. Mayyas, "A robust variable step-size lms-type algorithm: analysis and simulations," *IEEE Transactions on Signal Processing*, vol. 45, no. 3, pp. 631–639, Mar 1997.

[24] D. H. Dini and D. P. Mandic, "Widely linear modeling for frequency estimation in unbalanced three-phase power systems," *IEEE Transactions on Instrumentation and Measurement*, vol. 62, no. 2, pp. 353–363, Feb 2013.

[25] P. Sristi, W. S. Lu, and A. Antoniou, "A new variable-step-size lms algorithm and its application in subband adaptive filtering for echo cancellation," in *ISCAS 2001. The 2001 IEEE International Symposium on Circuits and Systems (Cat. No.01CH37196)*, vol. 2, May 2001, pp. 721–724 vol. 2.

[26] F. B. Costa, A. Monti, and S. C. Paiva, "Overcurrent protection in distribution systems with distributed generation based on the real-time boundary wavelet transform," *IEEE Transactions on Power Delivery*, vol. 32, no. 1, pp. 462–473, Feb 2017.

[27] Univ. Washington, "Power systems test washington, 2006," *WU*, 2006. [Online]. Available: https://www2.ee.washington.edu/research/pstca/

[28] Hydro-Quebec, *SimPowerSystem^{TM}, User's Guide (Second Generation*. MathWorks: ¡http://www.mathworks.com¿, 2013.

[29] N. Jenkins, R. Allan, P. Crossley, D. Kirschen, and G. Strbac, *Embedded generation*, first edition ed. The Institution of electrical engineers, IEE Power and Energy Series 31, ISBN 0852967748, Herts, United Kingdom, 2000.

[30] A. Samui and S. R. Samantaray, "Assessment of rocpad relay for islanding detection in distributed generation," *IEEE Transactions on Smart Grid*, vol. 2, no. 2, pp. 391–398, June 2011.

[31] "Ieee application guide for ieee std 1547(tm), ieee standard for interconnecting distributed resources with electric power systems," *IEEE Std 1547.2-2008*, pp. 1–217, 2009.

[32] M. Geidl, *Protection of Power Systems with Distributed Generation: State of the Art*, Power Systems Laboratory. Swiss Federal Institute of Technology (ETH) Zurich, 2005.

[33] *TMS320C6748™ Fixed- and Floating-Point DSP Datasheet*, Texas Instruments, 2009 [Revised 2017].